Experimental studies of lower hybrid wave propagation

P. M. Bellan and Miklos Porkolab

Plasma Physics Laboratory, Princeton University, Princeton, New Jersey 08540
(Received 18 December 1975)

Experimental measurement of the dispersion and damping of externally excited lower hybrid waves are presented. A multiple-ring slow-wave antenna, having $2\pi/k_z = 23$ cm, is used to excite these waves in the Princeton L3 or L4 linear devices ($B = 0.5$–2.8 kG uniform to $\pm$ 1% for 1.6 m, $n \approx 10^{10}$ cm^{-3}, $T_e \approx 3$–5 eV, $T_i \lesssim 0.1$ eV, He gas, plasma diameter approximately equal to 10 cm). The waves are localized in a spatial wave packet that propagates into the plasma along a conical trajectory which makes a small angle with respect to the confining magnetic field. Measurements of the dependence of wavelength on frequency are in good agreement with the cold plasma dispersion relation. Measured values of the wave damping are in good agreement with Landau damping by the combination of the main body of the electron distribution and an approximately 30% high energy ($T_e \approx 15$–30 eV) electron tail.

I. INTRODUCTION

Because of their potential for heating fusion reactors, lower hybrid waves have recently been the subject of considerable theoretical and experimental work. Stix[1] and Golant[2] showed theoretically that only waves having a k_z sufficiently large to satisfy the accessibility condition, $c^2k_z^2/\omega^2 > 1 + \omega_{pe}^2/\omega_{ce}^2$, can propagate from the edge of the plasma to the lower hybrid layer. (Here, ω_{pe} is the electron plasma frequency at the lower hybrid layer, ω_{ce} is the electron cyclotron frequency, c is the velocity of light, k_z is the component of k parallel to the confining magnetic field, and ω is the rf generator frequency.) It has been well known that cold plasma theory predicts that k_x, the component of k perpendicular to the confining magnetic field, should diverge at the lower hybrid layer. However, by including the lowest order hot plasma effects in the lower hybrid dispersion relation, Stix[3] showed that the divergence of k_x does not occur and that instead, the cold lower hybrid waves should convert linearly into a hot ion plasma mode near the lower hybrid layer. These converted hot ion plasma waves have never been observed experimentally.

The theories presented in Ref. 1, 2, and 3 deal with the behavior of a single Fourier mode having a specific k_z and k_x. Realistic, finite sources excite a spectrum of k_z modes so that the wave field of a finite source cannot be described directly by these theories. In order to understand what kind of cold plasma wave fields a particular finite source would excite, Kuehl[4] solved the problem of an oscillating point source in a plasma. He assumed that the point source acted as a delta function, and so excited a whole spectrum of k_z modes. The dispersion relation assigned a k_x to each k_z mode, so that there was also a corresponding spectrum of k_x modes. Superposing this spectrum of k_x, k_z modes, and inverse transforming the result to x, z space gave a field pattern completely different from what one's intuition would expect from simply looking at the dispersion relation. The field turned out to be *singular* along two lines lying in the x-z plane and intersecting the point source. The lines made a finite angle ($\theta \approx \omega/\omega_{pe}$, where ω is the wave frequency and ω_{pe} is the electron plasma frequency) with respect to the magnetic field. In regions other than these two lines, the field was zero. Fisher and Gould[5] have experimentally verified the existence of these lines for electron plasma waves and called them *the resonance cones.* We note that the origin of resonance cones can also be found in an earlier paper by Dawson and Oberman.[6] More recently, Briggs and Parker[7] showed that the lower hybrid waves (whose dispersion is the low frequency extension of the electron plasma wave dispersion) also propagate on resonance cones when excited by a dipole source. They also showed that near the lower hybrid layer the cone became nearly parallel to the confining magnetic field.

Thus, the results of Refs. 4, 5, and 7 show that a particular finite source, namely, the point source, does not excite waves having well-defined k_z and k_x. However, it would be worthwhile to excite such waves in order to make a quantitative experimental check of the wave dispersion relation. Hooke and Bernabei[8] attempted to excite well-defined waves by using a parallel plate source. However, Colestock and Getty[9] showed that such plates excite mainly resonance cones emanating from the ends of the plates, in agreement with our recent theory[10] and also with Ref. 6. In Ref. 10 we calculated the wave field excited by several types of extended wave sources and found that in order to excite waves with a well-defined k_x and k_z, it is necessary to use a source periodic in the z direction. We also showed how the cold plasma waves excited by a finite source would convert into hot ion plasma waves.

The present work is devoted to the experimental study of lower hybrid waves excited by a periodic source designed in accordance with our theory.[10] The plan of the paper is as follows: In Sec. II we will briefly discuss the lower hybrid dispersion relation, then give a summary of the theories of resonance cones and finite sources, and finally describe the mechanisms that could cause damping of lower hybrid waves. In Sec. III we will present experimental measurements of the dispersion of these waves (preliminary dispersion measurements have been presented in Ref. 11), and in Sec. IV we will present measurements of the wave damping. Because of strong damping observed near the lower hybrid layer, mode conversion into hot ion plasma waves was not observed. Finally, in Sec. V we will present a summary of this work.

II. REVIEW OF LOWER HYBRID WAVE PROPAGATION THEORY

A. Dispersion relation

Electrostatic lower hybrid modes are described by the dispersion relation

$$\frac{k_x^2}{k_z^2} = -\frac{K_{zz}}{K_{xx}} \tag{1}$$

which in the cold plasma limit reduces to

$$\frac{\omega^2}{\omega_{lh}^2} = 1 + \frac{m_i}{m_e}\frac{k_z^2}{k^2} \ . \tag{2}$$

Here, z and x denote directions parallel and perpendicular to the confining magnetic field; $K_{zz} = 1 - \omega_{pe}^2/\omega^2$; $K_{xx} = 1 - \omega_{pi}^2/\omega^2 + \omega_{pe}^2/\omega_{ce}^2$; $\omega_{lh}^{-2} = \omega_{pi}^{-2} + |\omega_{ci}\omega_{ce}|^{-1}$; ω_{pi}, ω_{pe} are the ion and electron plasma frequencies, ω_{ci}, ω_{ce} are the ion and electron cyclotron frequencies, and m_i, m_e are the ion and electron masses, respectively. Equations (1) and (2) hold for inhomogeneous as well as homogeneous plasmas, provided the WKB approximation is valid.

Let us now briefly review the main features of Eqs. (1) and (2). Evaluation of $\partial\omega/\partial k_x$ shows that the wave is backward in the x direction [i.e., $(\partial\omega/\partial k_x)(\omega/k_x) < 0$]. The dispersion relation also shows that, in the presence of a density gradient in the x direction, k_x increases as the wave propagates into regions of increasing plasma density. In particular, for a fixed k_z, k_x becomes very large when the wave reaches regions where the local lower hybrid frequency ω_{lh} is close to the wave frequency, ω. Near the lower hybrid layer, mode conversion can occur.[3]

B. Resonance cones

As we pointed out in the Introduction, finite sources excite a spectrum of k_z modes, and in particular, point sources excite resonance cones. In retrospect it is possible to show why resonance cones exist without going through all the complication of Fourier transformations. The dispersion relation for lower hybrid waves was obtained from Poisson's equation for a dielectric medium, namely,

$$\nabla \cdot \mathbf{K} \cdot \nabla\phi = 0. \tag{3}$$

In the lower hybrid parameter regime $\mathbf{K}$ is anisotropic and consists essentially of K_{xx} which is positive and K_{zz} which is negative. In a homogeneous plasma Eq. (3) becomes

$$\frac{\partial^2\phi}{\partial x^2} = \frac{|K_{zz}|}{K_{xx}}\frac{\partial^2\phi}{\partial z^2} \ . \tag{4}$$

This equation is formally the same as the familiar equation

$$\frac{\partial^2\psi}{\partial t^2} = c^2\frac{\partial^2\psi}{\partial z^2} \ , \tag{5}$$

except that x has replaced t and $|K_{zz}|/K_{xx}$ has replaced c^2. It is well known that solutions of Eq. (5) propagate along characteristics $z \pm ct$, so we can see that the solutions of Eq. (4) will similarly propagate along the characteristics $z \pm (|K_{zz}|/K_{xx})^{1/2}x$. These characteristics are precisely the resonance cones. Thus, we may conclude that a point source excites a singular disturbance which propagates along a resonance cone.[4,5,7] From the preceding discussion we can also see why a point source, such as a wire probe, will not excite waves having well defined, measurable k_x and k_z.

C. Periodic source theory

Because measurements of the wavelengths can provide a direct check of the dispersion relation, it is worthwhile to find a way of exciting waves with well-defined k_x and k_z. In addition, the accessibility condition of Stix[1] and Golant[2] shows that only waves having $(ck_z/\omega)^2 \gtrsim 1 + \omega_{pe}^2(x_{lh})/\omega_{ce}^2$ can propagate without reflection from the edge of the plasma to the lower hybrid layer. Thus, it is important to study the propagation of lower hybrid waves having a controlled, well defined and relatively narrow k_z spectrum.

In Ref. 10 we presented theoretical results which showed that a source periodic in the z direction will selectively excite a k_z corresponding to the periodicity. The waves excited by such a source, shown in Fig. 1, are spatially localized between conical trajectories emanating from the ends of the source. We note that the number of wavelengths existing in the plasma in both the x and z directions is the same as the number of wavelengths along the periodic source.

D. Theory of wave damping

In the present experiments the wave is being continuously driven by an external source so that damping appears as a spatial attenuation of the wave as it propagates radially into the plasma. This radial attenuation is equivalent to k_x having an imaginary component, k_{x_i}. The homogeneity of the plasma in the z direction and

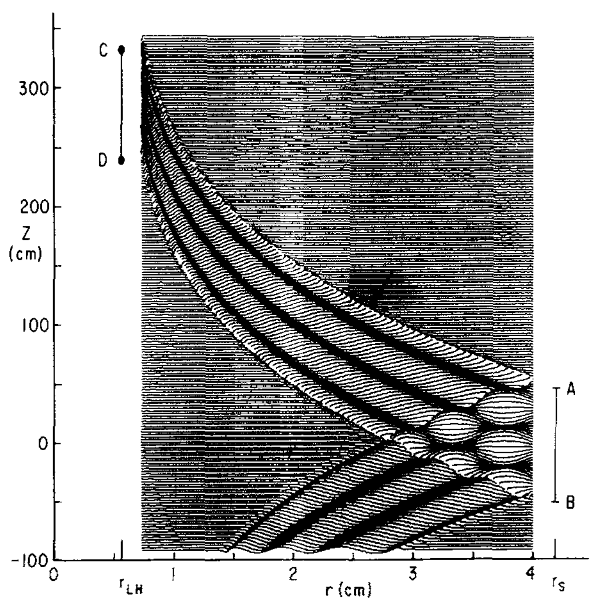

FIG. 1. Plots of field generated by a 100 cm long slow wave structure (located along AB). $\lambda_z = 33.3$ cm; density profile is Lorentzian, $n(r) = 10^{12}[1 + (r/0.75)^2]$; $f = 50$ MHz; $B = 2$ kG; He gas. Logarithmic singularities (arrow) bound the wave field.

the boundary conditions imposed by the source fix k_z, while the rf oscillator fixes ω. The relative importance of different damping mechanisms will be the same for homogeneous or inhomogeneous plasmas, as long as the WKB criterion is satisfied. Consequently, we may estimate the relative magnitudes of the various damping mechanisms by suitably modifying Eq. (1) to include dissipative effects. We will first briefly review how a dissipative term will modify Eq. (1) to give k_x an imaginary component, and we will then discuss how several different damping mechanisms contribute dissipative terms.

Equation (1) is a linear dispersion relation of the form

$$\epsilon(\omega, k_x, k_z) = \frac{k_x^2}{k^2} K_{xx} + \frac{k_z^2}{k^2} K_{zz} = 0. \tag{6}$$

Since ω and k_z are fixed as already mentioned, if ϵ has an imaginary part due to some damping mechanism, then as also mentioned here, k_x must become complex

$$k_x = k_{x_r} + ik_{x_i}. \tag{7}$$

If the damping is weak, then $k_{x_i}/k_{x_r} \ll 1$ and the dispersion relation may be written as

$$\epsilon(\omega, k_x, k_z) \simeq \epsilon_r(\omega, k_{x_r} + ik_{x_i}, k_z) + i\epsilon_i(\omega, k_{x_r}, k_z) = 0. \tag{8}$$

Taking real and imaginary parts of Eq. (8), we find that

$$\begin{aligned} &\epsilon_r(\omega, k_{x_r}, k_z) \simeq 0 \\ &k_{x_i} \simeq \frac{-\epsilon_i(\omega, k_{x_r}, k_z)}{\partial\epsilon_r/\partial k_x} \quad . \end{aligned} \tag{9}$$

Since it is more convenient to compare theory and experiment in terms of dimensionless quantities, we will express the damping in the form of the ratio

$$\frac{k_{x_i}}{k_{x_r}} = -\frac{1}{2}\,\frac{\epsilon_i(\omega, k_{x_r}, k_z)}{k_x^2\,\partial(\epsilon_r/\partial k_x^2\,)} = -\frac{1}{2}\,\frac{\epsilon_i(\omega, k_{x_r}, k_z)}{\partial(k_x^2\epsilon_r)/\partial k_x^2} \quad . \tag{10}$$

Qualitatively, $k_{x_i}/k_{x_r} = (2n\pi)^{-1}$ means that the wave e folds in n wavelengths. Using the fact that for $\omega \ll \min(\omega_{pe}, \omega_{ce})$, we have $k_x^2 \simeq k^2$ and

$$\epsilon_r \simeq \frac{k_{x_r}^2}{k^2} K_{xx} + \frac{k_z^2}{k^2} K_{zz} \simeq 0, \tag{11}$$

so that Eq. (10) may be written as

$$\frac{k_{x_i}}{k_{x_r}} = \frac{-k^2}{2k_{x_r}^2}\,\frac{\epsilon_i(\omega, k_{x_r}, k_z)}{K_{xx}} = \frac{k^2}{2k_z^2}\,\frac{\epsilon_i(\omega, k_{x_r}, k_z)}{K_{zz}} \quad . \tag{12}$$

We see that the ratio k_{x_i}/k_{x_r} is not directly affected by the lower hybrid resonance unless $k^2\epsilon_i$ is proportional to some positive power of k_x.

E. Summary of most probable damping mechanisms

1. Collisional damping

With the inclusion of collisions we find

$$K_{xx} = 1 - \frac{\omega_{pi}^2}{\omega^2(1 + i\nu_i/\omega)} - \frac{\omega_{pe}^2/(1 + i\nu_e/\omega)}{\omega^2 - \omega_{ce}^2/(1 + i\nu_e/\omega)^2}\,,$$

and

$$K_{zz} = 1 - \frac{\omega_{pi}^2}{\omega^2(1 + i\nu_i/\omega)} - \frac{\omega_{pe}^2}{\omega^2(1 + i\nu_e/\omega)} \quad , \tag{13}$$

where ν_i is the larger of the ion–neutral and ion–electron collision frequencies, while ν_e is the larger of the electron–neutral and electron–ion collision frequencies. In this case

$$\epsilon_i = \frac{\omega_{pi}^2}{\omega^2}\,\frac{\nu_i}{\omega} + \frac{k_x^2}{k^2}\,\frac{\omega_{pe}^2}{\omega_{ce}^2}\,\frac{\nu_e}{\omega} + \frac{k_z^2}{k^2}\,\frac{\omega_{pe}^2}{\omega^2}\,\frac{\nu_e}{\omega}\,, \tag{14}$$

and since $k_x^2/k^2 \simeq 1$, using Eq. (12) we have

$$\frac{k_{x_i}}{k_{x_r}} = \frac{k^2}{2k_z^2 K_{zz}} \left(\frac{\omega_{pi}^2}{\omega^2}\,\frac{\nu_i}{\omega} + \frac{\omega_{pe}^2}{\omega_{ce}^2}\,\frac{\nu_e}{\omega} + \frac{k_z^2}{k^2}\,\frac{\omega_{pe}^2}{\omega^2}\,\frac{\nu_e}{\omega} \right). \tag{15}$$

2. Electron Landau damping

The dispersion relation with electron Landau damping included is

$$\frac{k_x^2}{k^2} K_{xx} + \frac{k_z^2}{k^2} K_{zz} + \frac{i\pi^{1/2}}{k^2\lambda_D^2}\,\frac{\omega}{k_z v_{T_e}} \exp\left(-\frac{\omega^2}{k_z^2 v_{T_e}^2}\right) = 0, \tag{16}$$

where

$$\lambda_D = \left(\frac{\kappa T_e}{m_e}\right)^{1/2} \frac{1}{\omega_{pe}} \tag{17}$$

is the electron Debye length, and

$$v_{T_e} = (2\kappa T_e/m_e)^{1/2} \tag{18}$$

is the electron thermal velocity (here, κ is Boltzmann's constant, and T_e is the electron temperature). In this case we have

$$\epsilon_i = \frac{\pi^{1/2}}{k^2\lambda_D^2}\,\frac{\omega}{k_z v_{T_e}} \exp\left(-\frac{\omega^2}{k_z^2 v_{T_e}^2}\right) \tag{19}$$

and

$$\frac{k_{x_i}}{k_{x_r}} = \frac{\pi^{1/2}}{2k_z^2 K_{zz}\lambda_D^2}\,\frac{\omega}{k_z v_{T_e}} \exp\left(-\frac{\omega^2}{k_z^2 v_{T_e}^2}\right). \tag{20}$$

Noting that $K_{zz} \simeq -\omega_{pe}^2/\omega^2$ and $\lambda_D^{-1} = \sqrt{2}\,\omega_{pe}/v_{T_e}$, Eq. (20) may be written as

$$\frac{k_{x_i}}{k_{x_r}} = -\pi^{1/2}\left(\frac{\omega}{k_z v_{T_e}}\right)^3 \exp\left(-\frac{\omega^2}{k_z^2 v_{T_e}^2}\right) \tag{21}$$

which is independent of plasma density or ion mass.

If a high energy tail were present having electron thermal velocity v'_{T_e} and density n', then the additional Landau damping due to the tail would be

$$\frac{k_{x_i}}{k_{x_r}} = -\pi^{1/2}\,\frac{n'}{n}\left(\frac{\omega}{k_z v'_{T_e}}\right)^3 \exp\left(-\frac{\omega^2}{k_z^2 v_{T_e}'^2}\right). \tag{22}$$

We note that the tail may have a large effect on ϵ_i if $\omega/k_z \approx v'_T$, but only a small effect on ϵ_r if $n'/n \ll 1$. Thus, a tail containing a small fraction of the total electrons can cause a substantial damping and yet not affect the real part of the dispersion. If the tail density is expressed as a fraction α of the total density, then the damping from the combination of the main body and tail is

$$\frac{k_{x_i}}{k_{x_r}} = -\pi^{1/2}\left[(1-\alpha)\left(\frac{\omega}{k_z v_{T_e}}\right)^3 \exp\left(-\frac{\omega^2}{k_z^2 v_{T_e}^2}\right) + \alpha\left(\frac{\omega}{k_z v'_{T_e}}\right)^3 \exp\left(-\frac{\omega^2}{k_z^2 v_{T_e}'^2}\right)\right]. \tag{23}$$

3. *Turbulent damping*

The theories of turbulent damping are complex and not generally agreed upon. The existing theories deal with low frequency turbulence, $\omega_t \approx$ drift or acoustic wave frequencies, or with high frequency turbulence, $\omega_t \approx \omega$ (here, ω_t is the characteristic frequency of the turbulence). Dupree[12] has treated the low frequency turbulence and has shown analytically how turbulence-induced damping can cause a nonlinear saturation of the drift wave instability. Okuda and Dawson,[13] and Chu[14] have treated high frequency turbulence using numerical particle simulation techniques and have shown that lower hybrid waves can be damped by high frequency turbulence ($\omega_t \approx \omega_{lh}$). However, their computer model differs from our experimental situation in that they set $k_z = 0$.

In Refs. 12–14 it is shown that turbulence causes an anomalous diffusion which, in turn, gives a damping. In Ref. 12 this turbulence-induced diffusion was derived using particle orbit calculations and the resulting diffusion coefficient was found to be

$$D_\perp \sim c(\langle \phi_t^2 \rangle^{1/2}/B) \tag{24}$$

where ϕ_t is the turbulent potential fluctuation. On the other hand, in Refs. 13 and 14 it was possible to simply measure the actual diffusion of the particles in the simulations, and then with this measurement calculate the diffusion coefficient. Since the wave damping turns out to be a function of $D_\perp$, and not the mechanism producing $D_\perp$, we may split the problem into (i) calculating how a given $D_\perp$ causes damping, and (ii) calculating or measuring $D_\perp$.

In Refs. 13 and 14 it has been shown that with the inclusion of perpendicular diffusion, the linearized equation of motion becomes

$$\frac{\partial \mathbf{v}_\sigma}{\partial t} = \frac{q_\sigma}{m_\sigma}\left(-\nabla\phi + \frac{\mathbf{v}_\sigma \times \mathbf{B}}{c}\right) + D_\perp \nabla^2 \mathbf{v}_{\sigma_\perp}. \tag{25}$$

(We have assumed that the diffusion and viscosity magnitudes are the same.) After the usual Fourier analysis, the additional term is observed to be approximately equivalent to an effective collision frequency, $\nu_{ef} \approx k_x^2 D_\perp$. By using the dispersion relation found from Eq. (25), Poisson's equation and the equation of continuity, we find that

$$\epsilon_i = \frac{1}{k^2}\left(k_x^4 \frac{\omega_{pi}^2}{\omega^2}\frac{D_{\perp i}}{\omega} + k_x^4 \frac{\omega_{pe}^2}{\omega_{ce}^2}\frac{D_{\perp e}}{\omega}\right). \tag{26}$$

Substituting Eq. (26) in Eq. (12), we find that

$$\frac{k_{x_i}}{k_{x_r}} = \frac{1}{2k_z^2 K_{zz}}\left(k_x^4 \frac{\omega_{pi}^2}{\omega^2}\frac{D_{\perp i}}{\omega} + k_x^4 \frac{\omega_{pe}^2}{\omega_{ce}^2}\frac{D_{\perp e}}{\omega}\right). \tag{27}$$

III. EXPERIMENTAL MEASUREMENTS OF THE WAVE DISPERSION

The experiments were done using the Princeton L3 and L4 machines, both linear devices having a 160 cm long uniform (to ±1%) magnetic field. The field of the L4 machine was bounded on both ends by a 1.8:1 mirror field while L3 had an adjustable mirror field.

During the course of our experiments we found that, in order to carry out quantitative measurements of these waves, it was important to have a source with minimal density fluctuations. This is because background density fluctuations cause a phase decorrelation of the wave, which makes interferometric measurements difficult or impossible. We thus used four different plasma sources and found that either a hot cathode discharge source[15] or a multiple filament and dipole magnet source[16] produced suitable plasmas, while high power rf discharges, such as Lisitano coils[17] or a coaxial rf source produced plasmas with excessive amounts of density fluctuations. (The coaxial rf source consisted of a 7.5 cm diam rigid 50 Ω coax, coaxial with the magnetic field and open circuited inside the vacuum chamber. This source was powered by a 1 kW, 450 MHz oscillator and produced a plasma similar to that of the Lisitano coil.)

We designed a periodic slow wave antenna in accordance with the requirements of Ref. 10 so that periodic waves would be linearly excited in the plasma. (We note that lower hybrid waves have been previously excited nonlinearly, by parametric decay.[18,19]) The antenna, which is shown in Fig. 2, consisted of an array of rings surrounding the plasma, with the rings having an outside diameter slightly less than that of the L4 vacuum chamber. In order to satisfy both the electrostatic approximation and yet avoid excessive Landau damping, our structure had to have a parallel wavelength $2\pi/k_z$, satisfying

$$v_{T_e} \ll \omega/k_z \ll c. \tag{28}$$

The helium (or occasionally hydrogen) plasmas with which we worked typically had temperatures $T_e \simeq 5$ eV, densities of 5×10^9–2×10^{10}, diameters of ≈10 cm, and were confined by magnetic fields of 0.5–2.8 kG. We spaced the rings on the antenna to have $2\pi/k_z = \lambda_z = 23$ cm so that lower hybrid waves propagating in the

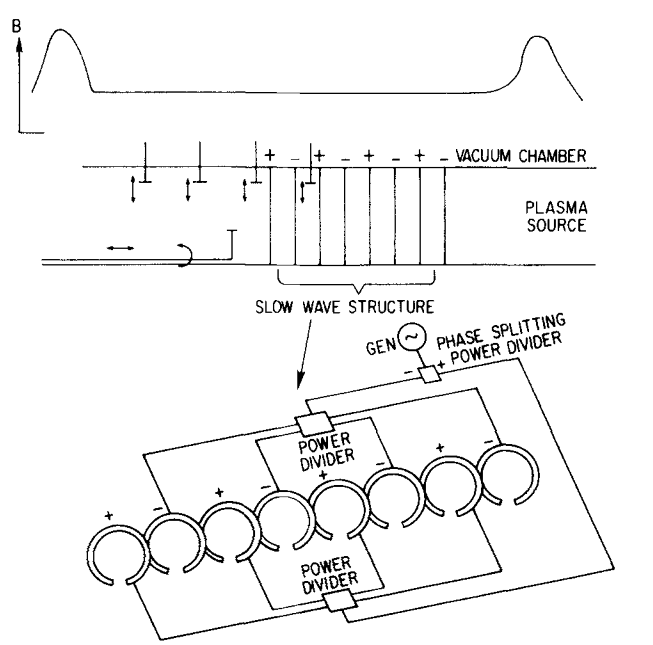

FIG. 2. Experimental setup. The eight rings driven by power dividers alternate in phase by 180°.

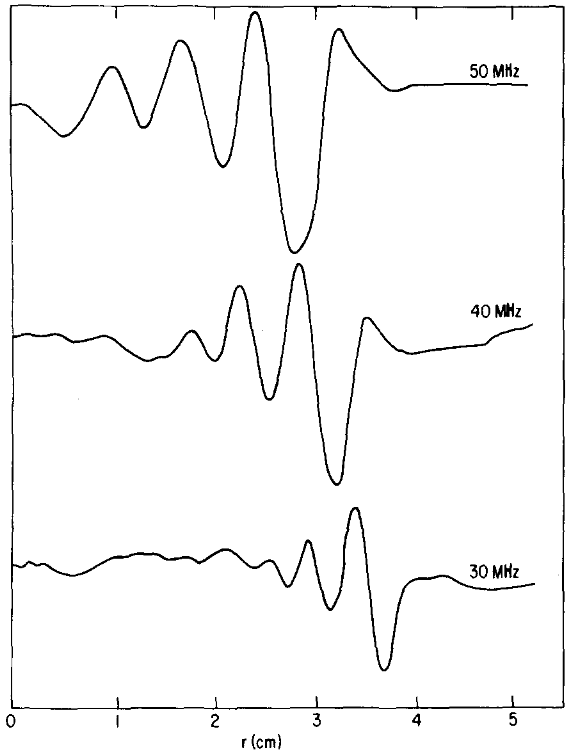

FIG. 3. Typical radial probe interferometer traces for a few frequencies. Note how both the wave packet moves out of the plasma and the wavelength decreases as the frequency is lowered. The probe is 30 cm beyond the last ring of the slow wave structure.

plasma (these waves have $\omega \gtrsim \omega_{lh}$) would satisfy Eq. (28) for the range of frequencies 10 to 100 MHz. We compromised on a total length of four wavelengths (92 cm) for the structure. This choice gave sufficient wavelengths to allow us to check the theoretical prediction that the number of waves in the plasma equals the number on the source, and yet was short enough to leave adequate room for the waves to propagate in a reasonably long uniform field region beyond the source (cf. Fig. 2). The rings making up the periodic array had slots cut in their bottoms so as to allow an axial probe to pass through. Using a power divider having two outputs of opposite phase (cf. Fig. 2), the eight rings were periodically phased $+-+-$, etc. An rf oscillator was connected to the input of the power divider and the two outputs were each connected to a four-way power divider which, in turn, was connected to four of the rings.

Up to three radial probes were positioned at different axial positions from the slow wave structure. We also constructed an axial probe that could be rotated about its axis so that axial measurements could be made at different radial positions (or radial measurements at arbitrary axial positions). The probe signal was fed into a standard interferometer circuit. The cables to the various probes and the cable in the reference leg of the interferometer were of the same length so that the relative phase between the probes and the reference signal would not have any instrumental frequency dependence coming from phase shifts along the cables. The interferometer output was displayed on an $x-y$ recorder.

In Fig. 3 we show typical interferometer output traces obtained with a radial probe. As predicted in Ref. 10 (and also shown in Fig. 1), the number of wavelengths in the wave packet (four in this case) corresponds to the number of wavelengths on the periodic source. At lower frequencies the wave packet is farther from the plasma center, in agreement with the cone trajectory $z = g(x)$, which implies that the cone angle, $\theta \approx O(\omega/\omega_{pe})$, is approximately proportional to wave frequency. In Fig. 4 we show a series of axial probe interferometer signals. The bottom trace shows the four wavelength long field of the source while the

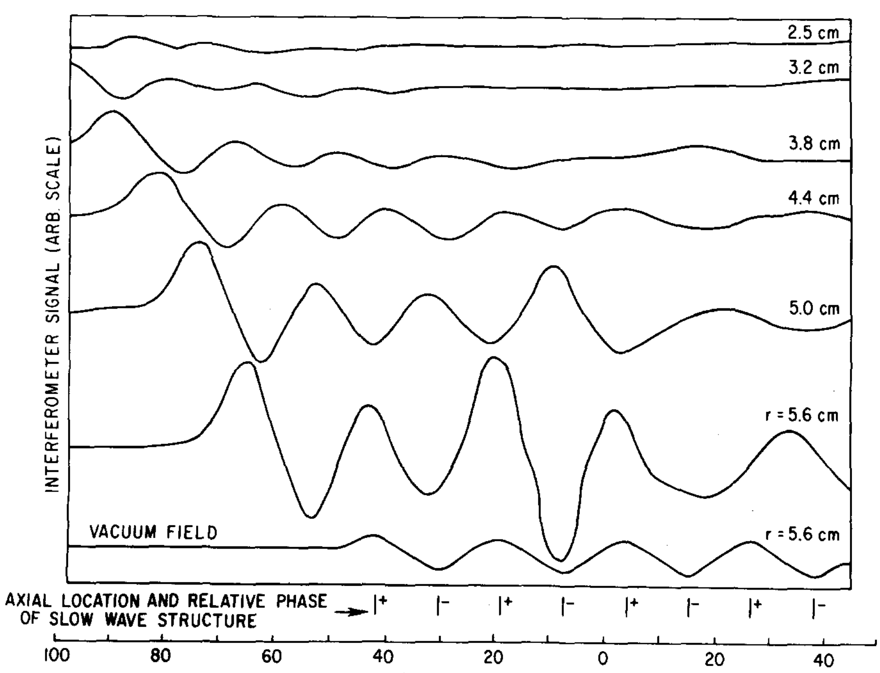

FIG. 4. Axial probe interferometer signal. The axial traces made at different radial positions, r, show the conical trajectory of the wave. The bottom trace is the vacuum field of the slow wave structure. He gas.

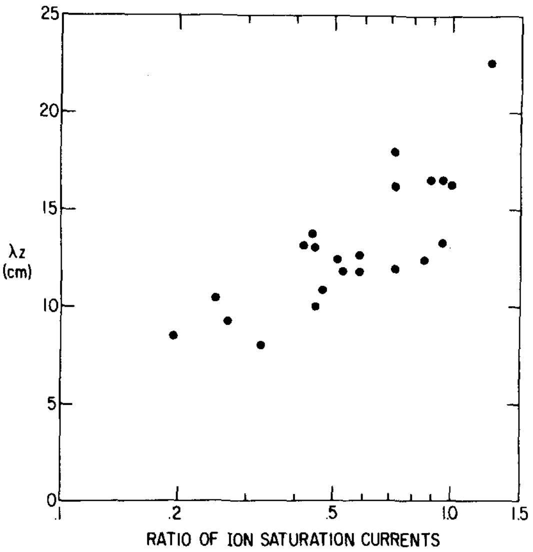

FIG. 5. λ_z vs the ratio of the ion saturation currents from two probes separated axially by 150 cm. These measurements were obtained by varying the filling pressure and/or the mirror field.

other traces show waves in the plasma at different radial positions. The conical trajectory of the waves is apparent in these traces. We also note that k_z is constant, and is fixed by the boundary condition imposed by the periodicity of the source.

We found that k_z was only constant when the axial density gradient was small. For large axial density gradients, k_z would increase as the density decreased axially. We note that this is the opposite of the behavior of k_x when there is a radial density gradient and k_z is fixed. However, this behavior is in agreement with the dispersion relation, Eq. (1), for the following reason: Since k_x occurs in the numerator of Eq. (10) while k_z occurs in the denominator, we may expect k_z to behave in the opposite way compared with k_x when there is a change in plasma parameters. (Which one of k_x or k_z remains fixed, while the other varies, depends on whether the plasma is uniform radially or axially.) The axial density gradient existed mainly in the slow wave structure and was monitored in a semi-quantitative way using two similar Langmuir probes, one on each end of the slow wave structure. The axial separation of the probes was 150 cm and both probes were located on-axis. We found that the axial scale length, calculated by assuming an exponential density decay over the distance between the two probes, decreased with increasing filling pressure. This scale length typically varied from approximately 10^3 cm at 0.5 μ to approximately 10^2 cm at 3 μ. In the former case, k_z was constant, while in the latter case k_z increased to about twice its initial value at the slow wave structure. The mirror field strength also affected the axial gradient, with the scale length generally decreasing with increasing mirror field. In Fig. 5 we show the variation of $\lambda_z = 2\pi/k_z$ with the ratio of ion saturation currents obtained from the two probes.

At higher pressures ($p \sim 3\ \mu$) where $\lambda_z \approx 10$–12 cm (instead of the 23 cm periodicity of the slow wave structure), we observed perpendicular wavelengths as short as 0.2 cm. At lower pressures ($p \approx 0.5\ \mu$) where $\lambda_z \approx 23$ cm, we found that the minimum observable perpendicular wavelength was approximately 0.4 cm. These investigations of the effect of axial density gradients were done using the multiple filament plasma source.[16]

In Figs. 6 and 7, and again in Figs. 8 and 9, we show a series of radial traces of the interferometer signal and wave amplitude for two wave frequencies, respectively. These measurements were made by rotating the axial probe at a sequence of axial positions. The axial probe had a double tip, which will be described in Sec. IV. Here again, we see the conical wave packet propagation and the fact that the waves in the plasma are an image of those on the source in agreement with the theoretical prediction presented in Fig. 1. Note in Fig. 6 the shortening of the wavelengths toward the plasma center. This is due to the increasing density, and the local wavelengths are in good agreement with WKB theory. In Figs. 6 and 7 the wave frequency was relatively high and the waves were weakly damped, while in Figs. 8 and 9 the wave frequency was relatively low and the wave was more strongly damped. From Figs. 8 and 9 it can be seen that the interferometer signal damps before the amplitude signal, indicating that a phase decorrelation is occurring. We will discuss the cause of such a decorrelation in the next section. From Figs. 7 and 9 we see that for each frequency there is a critical layer at

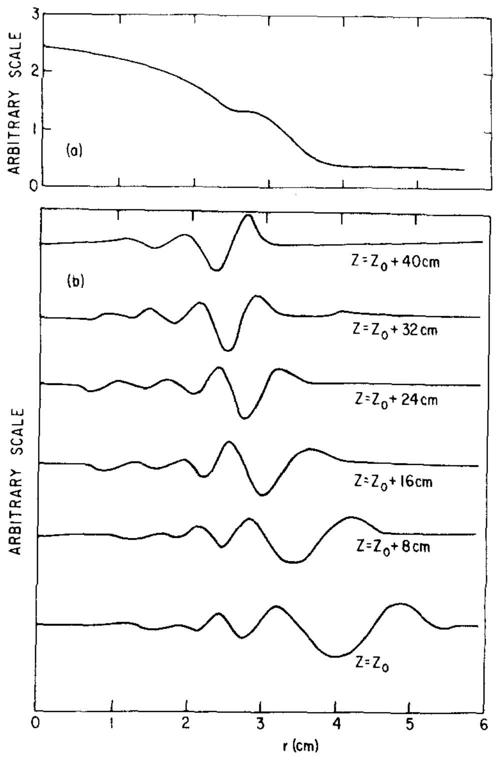

FIG. 6. (a) Density profile for (b) and Figs. 7–9. (b) Interferometer signal of radial wave field for a sequence of axial positions. The conical trajectory of the wave packet is in good agreement with the theory (cf. Fig. 1). He gas, $B = 1.3$ kG, $f = 20$ MHz.

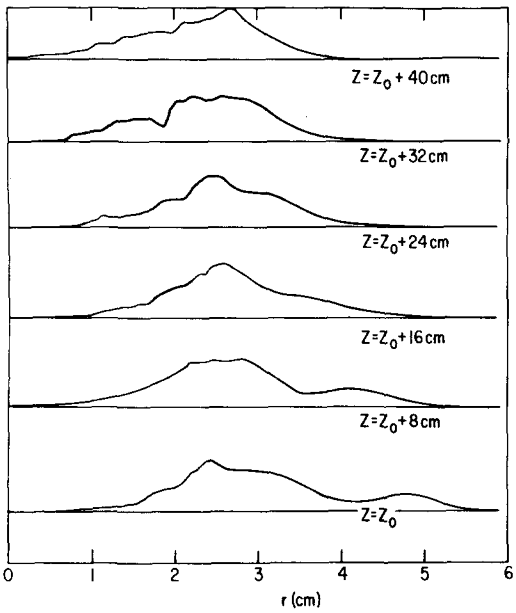

FIG. 7. Measurements of the wave electric field *amplitude* for the same conditions as Fig. 6. Note that the wave amplitude begins to damp at $r \approx 2.5$ cm regardless of axial position.

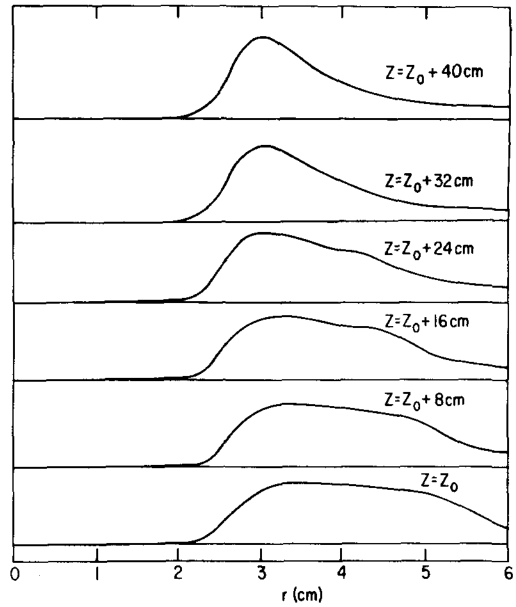

FIG. 9. Same as Fig. 7 except $f = 12$ MHz. The wave amplitude extends farther into the plasma than the interferometer signal (Fig. 8) would indicate. The wave packet moves along the conical trajectory up to a critical radial position where it is strongly damped.

which the wave amplitude is damped. In particular, it can be seen in Fig. 9 that the wave packet moves inward along the conical trajectory to about $r = 2.5$ cm, at which point strong damping takes place. This occurs because the wave damping is characterized by an inverse damping length, k_{x_i}, which is proportional to k_{x_r} which increases to large values near $r = 2.5$ cm. We note from Fig. 9 that since the wave packet is both moving inward along the conical trajectory and damping out at $r \approx 2.5$ cm, the radial width of the wave packet decreases with increasing axial displacement from the antenna. These measurements were made using a double-tipped rf probe (described in Sec. IV).

By using sampling techniques to measure the phase and group velocities directly, we have verified that the waves were "backward" [i.e., $(\partial\omega/\partial k_x)(\omega/k_x) < 0$]. As shown in the sampling circuit sketched in Fig. 10, an electronic switch was used to form temporal wave

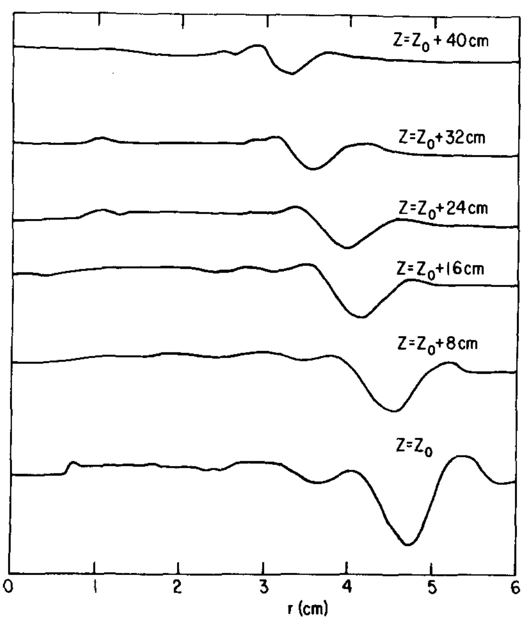

FIG. 8. Same as Fig. 6(b), except $f = 12$ MHz. The wave packet is radially farther out than the 20 MHz case and appears to be more strongly damped. This apparent damping comes from phase decorrelation (cf. Fig. 9 and discussion in text).

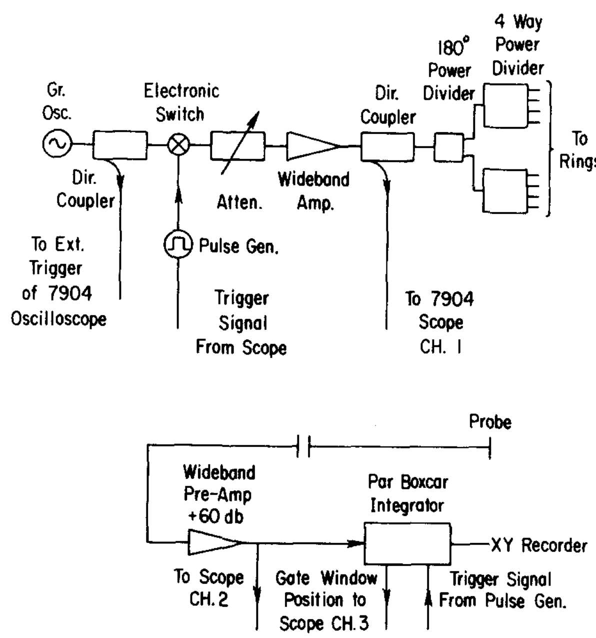

FIG. 10. Boxcar integrator sampling circuit. This circuit permitted direct observation of the direction of both the wave phase velocity and group velocity.

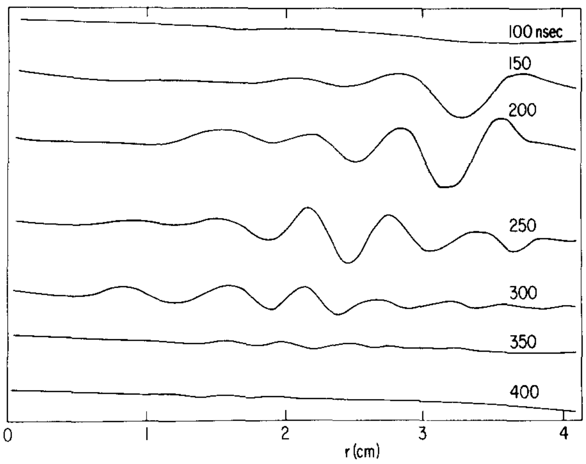

FIG. 11. Radial motion of wave packet using the boxcar integrator circuit. The wave packet moves radially into the plasma with increased time. $f = 40$ MHz.

packets (duration approximately 2–100 wave periods), which were then applied to the slow wave antenna. The resulting signal in the plasma was picked up by a probe and was sampled by a boxcar integrator at a sequence of times after the wave packet emission. These delayed observation times had to be synchronized with respect to the rf wave so that the wave phase coherence would be retained. This was achieved by triggering the electronic switch and the boxcar integrator simultaneously by a high speed oscilloscope (Tektronix 7904). The oscilloscope was set to sweep at the repetition rate desired for the wave packet and then was itself externally triggered by part of the rf oscillator signal so that the wave packet envelope would be phase coherent with the wave itself. The boxcar gate window was adjusted to be much shorter than the wave period so that the actual high frequency rf signal could be observed at a particular delay time. In Fig. 11 we see how the wave packet moves into the

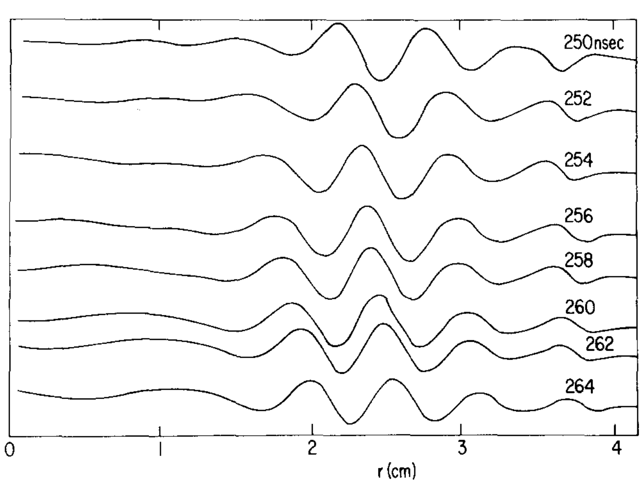

FIG. 12. Radial motion of the wave phase using the boxcar integrator circuit, same settings as Fig. 11 except that the time between successive traces is now much less a wave period. The wave phase moves radially out of the plasma with increased time.

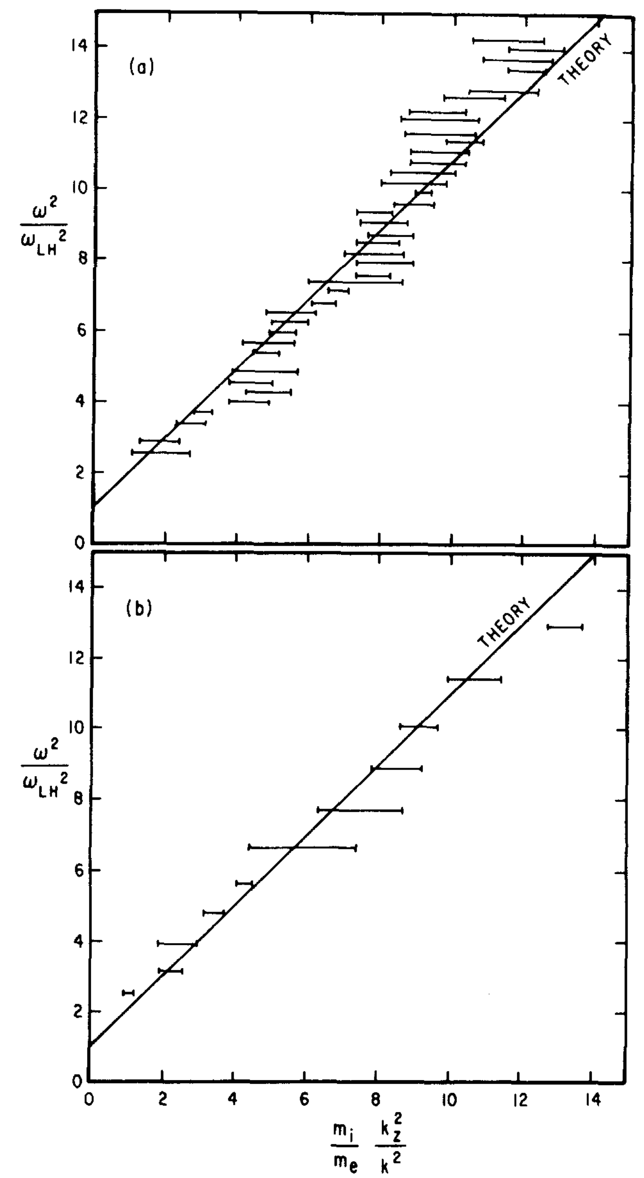

FIG. 13. (a) Comparison of experimental measurements of dependence of k_x on ω with Eq. (2); He plasma produced by coaxial rf source, $\lambda_z = 23$ cm; $B = 2470$ G; and fitted $n = 1.6 \times 10^{10}$ cm^{-3}. (b) Same as (a) except that hot cathode plasma data used. $\lambda_z = 23$ cm, $B = 515$ G, $n = 2.5 \times 10^9$ cm^{-3}.

plasma with increased time, while in Fig. 12 (made using 2 nsec time steps instead of the 50 nsec time steps of Fig. 11) we see how the wave phase moves out of the plasma.

We produced rf and hot cathode discharge plasmas that were uniform to ±10% radially, and then measured the dependence of radial wavelength on generator frequency. The results of these measurements are shown in Figs. 13(a) and 13(b) and compared with the theoretical dispersion relation Eq. (2). Of the parameters n, B, m_e/m_i, k_z, k_x, and ω occurring in the dispersion relation, only the density could not be measured accurately, and so we adjusted this parameter to give the best fit to the experimental data. The fitted density was in reasonable agreement with Langmuir probe measurements, using the theory of Laframboise.[20]

IV. MEASUREMENTS OF THE WAVE ATTENUATION

Spatial wave damping is customarily determined experimentally by measuring the e-folding distance of the interferometer signal envelope. We found that this method indicated a very strong wave damping, the magnitude of which appeared to be related to the density fluctuation level. Because the density fluctuation level varied from one plasma source to another, we found that for each source there was a typical minimum observable wavelength. For plasmas produced by the Lisitano coil or the coaxial rf source, no waves were observable when $n_e \approx 10^{12}$ cm^{-3} (and $\delta n/n$ was very large), and when these sources were operated at $n_e \approx 10^{10}$ cm^{-3} the minimum observable perpendicular wavelengths were approximately 9–10 mm. For the hot cathode discharge the minimum observable wavelength was approximately 4 mm, and for the multiple filament source approximately 2–4 mm.

However, it became apparent that measuring wave damping from the interferometer signal envelope was incorrect for the following reason. Interferometry requires that the measured wave be phase coherent with respect to a reference signal; if not, no wave will be observed. We found that as the lower hybrid wave propagated through the plasma, it lost coherence with respect to the reference signal (obtained from part of the transmitter signal). Consequently, the interferometer signal was attenuated because of this phase decorrelation, rather than because of a true dissipative damping of the wave. This decorrelation increased as the wavelength decreased.

The existence of such a decorrelation was verified by using a second stationary probe as the reference. When the reference probe was located near the receiving probe, a large coherent interferometer signal was often observed even if both the signals at the reference and pickup probes were decorrelated with respect to the transmitter. We also found that this damping due to phase decorrelation could be increased by injecting noise into a grid in the plasma.

The consequence of this confusing instrumental problem is that in the presence of background fluctuations one cannot safely use the interferometer signal envelope to measure lower hybrid wave damping. We therefore made measurements of the detected wave amplitude which, unlike the interferometer signal, is phase insensitive. However, with this technique one measures a "dc" signal (i.e., the wave amplitude) superimposed on a background of noise, modes other than lower hybrid waves, and stray pickup. These unwanted signals cause an uncertainty in the base line, making quantitative measurements of the wave amplitude difficult. In particular, we found that a standard T probe would pick up, in addition to the lower hybrid signal, a long wavelength signal consisting of the fast electromagnetic mode, and also what appeared to be natural resonances of the plasma column.[21] The amplitude of this additional signal was typically $0.1 \approx 0.3$ the lower hybrid wave amplitude, and consequently made it impossible to establish the baseline needed to calculate the damping of the lower hybrid wave amplitude. In

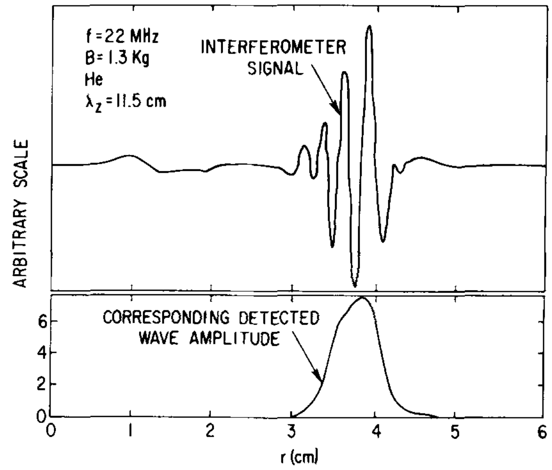

FIG. 14. Bottom: Typical amplitude signal measured using a double tipped rf probe as described in Sec. IV (high pressure equilibrium; $\lambda_z = 11.5$ cm). Top: interferometer trace of the same signal.

order to avoid picking up this undesirable long wavelength signal, we built a special double-tipped rf probe that measured the wave radial electric field (instead of the wave potential measured by a standard single-tipped T probe). This double probe consisted of two parallel lengths of 0.6 mm diam rigid coaxial cable, each having 5 mm of the center conductor exposed to act as a probe tip. The two tips were parallel to **B** and were spaced 1 mm apart. The outer conductors of the cables were soldered together and sprayed with boron nitride insulation. The subtraction of the signals coming from the two tips, which is required to obtain the electric field, was performed by a 180° phase reversing, wideband power divider. With this technique the long wavelength signals were rejected relative to the short wavelength lower hybrid wave, so that when the probe traveled outside the lower hybrid wave packet, the received signal went to zero.

Standard crystal detectors were not suitable for amplitude measurements because of their inherently nonlinear response. Instead, we tuned a spectrum analyzer to fixed frequencies (rather than having it scan frequencies) and used it in the linear response mode so that it effectively became a tuned rf voltmeter. We also electronically chopped the transmitted signal and used a lock-in amplifier, synchronized to the chopping frequency to reject random noise in the received signal. The cable from the probe to the spectrum analyzer was double shielded to reduce pickup of the transmitted signal due to stray capacitative coupling from outside the machine. Using these techniques, we were able to obtain an amplitude signal with a well-defined baseline and so were able to measure the e-folding of the lower hybrid wave amplitude.

Measurements of k_{x_i}/k_{x_r} were thus made by using the interferometer signal to determine k_{x_r}, and the e-folding of the amplitude signal to determine k_{x_i}. A typical amplitude signal, measured using the methods described here, is shown in Fig. 14, together with the corresponding interferometer signal. For low frequen-

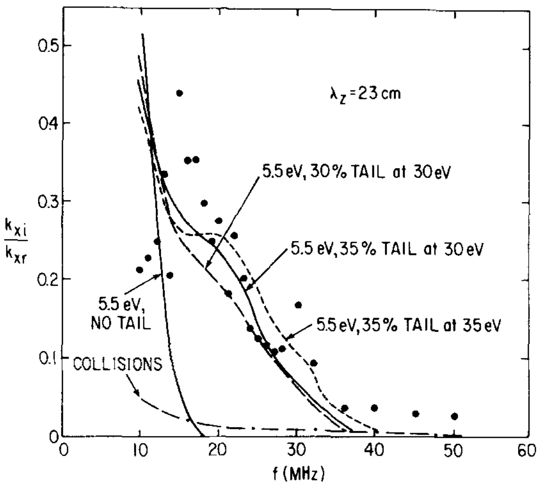

FIG. 15. Damping ratio k_{x_i}/k_{x_r} for the low pressure ($p \sim 0.5\ \mu$) equilibrium, He, $B = 1.3$ kG, $\lambda_z = 23$ cm. Data (dots) are in reasonable agreement with Landau damping from an electron distribution function having a 5.5 eV main body and an apmately 30%, 30 eV tail.

cy, short wavelength waves the interferometer signal was washed out due to phase decorrelation and k_{x_r} was determined from the dispersion relation, Eq. (1). In these cases the density used in Eq. (1) was calculated from measurements made at higher frequencies, where the longer wavelengths were less affected by phase decorrelation.

Using the method described here, we measured the damping ratio k_{x_i}/k_{x_r} over sequences of wave frequencies for two general types of equilibria, namely, low pressure ($p \approx 0.5\ \mu$) where $\lambda_z \approx 23$ cm, and high pressure ($p \approx 3\ \mu$), where $\lambda_z \approx 11.5$ cm. These measurements are plotted in Figs. 15 and 16, where we also show the k_{x_i}/k_{x_r} predicted by Landau damping with and without a high energy tail, and also collisional damping. (Collisions with neutrals are dominant here.)

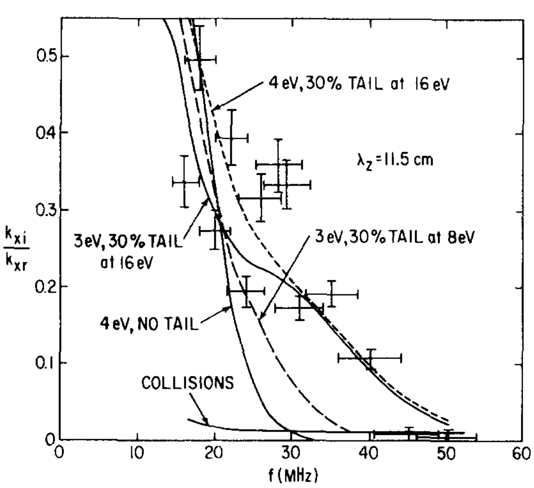

FIG. 16. Damping ratio k_{x_i}/k_{x_r} for the high pressure ($p \sim 3\ \mu$) equilibrium; He, $B = 1.3$ kG, $\lambda_z = 11.5$ cm. Data (⊢I⊣) are in reasonable agreement with the Landau damping from an electron distribution function having a 4 eV main body and an approximately 30%, 16 eV tail.

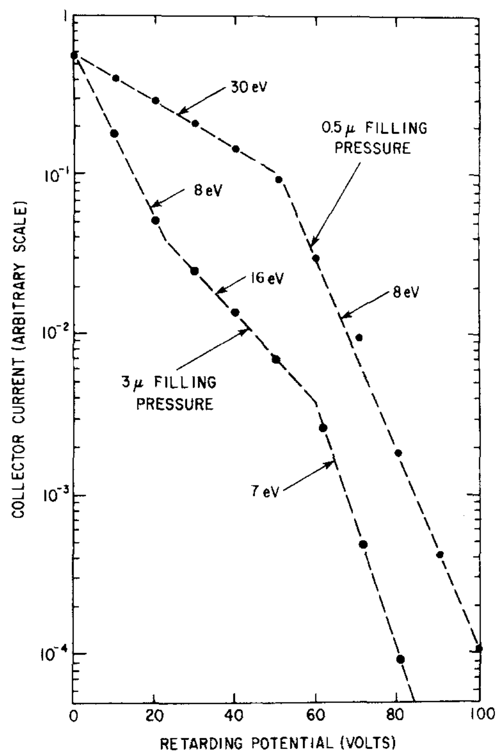

FIG. 17. Typical energy analyzer characteristics for both the low and the high pressure equilibria.

The theoretical curves were evaluated using Eqs. (15), (21), and (23), and values of $\nu_i = 10^6$ sec^{-1} and $\nu_e = 5 \times 10^6$ sec^{-1} were used. The main body temperature of 5.5 eV, used in the low pressure case, Fig. 15, was determined from Langmuir probe measurements. In the high pressure case Langmuir probe measurements indicated a main body temperature of 3 eV; we found better agreement between theory and experiment using 4 eV. In Fig. 16 damping for both 3 and 4 eV temperatures are plotted. As can be seen from the figures, neither collisional damping nor Landau damping from the main body alone is sufficient to account for the observed damping. However, both the Langmuir probe and a parallel electron energy analyzer showed that a high energy tail existed in the plasma. For the low pressure equilibrium, Langmuir probe measurements indicated tail temperatures of 20 eV while the energy analyzer (more reliable for tail measurements) gave approximately 30 eV for a range of energies up to about 60 V. (We note that the energy analyzer only detects the tail; it does not pick up the main body.)

For the high pressure equilibrium, the Langmuir probe characteristic indicated tail temperatures of 15–20 eV while the more reliable energy analyzer gave 8–16 eV. Typical energy analyzer characteristics for both the low and high pressure equilibria are shown in Fig. 17. From the Langmuir probe characteristics it appeared that the tail population was 20%–30% of the main body population; however, this is only a rough estimate because of the uncertainty in the location of the plasma potential.

We thus used, in Figs. 15 and 16, main body temperatures and tail temperatures that were in reasonable agreement with the probe measurements, and then chose tail percentages to give the best fit to the experimental data. We found that tail percentages of approximately 30% gave the best agreement. Since this is a reasonable percentage, we conclude that Landau damping from the combination of main body and tail is the mechanism causing damping of the wave.

The strong damping observed in Fig. 9 is an example of the occurrence of this Landau damping. As discussed in Sec. III, the damping occurs at a sharply defined radial position because Eqs. (21) and (23) show that k_{x_i} is proportional to k_{x_r}, and k_{x_r} is increasing as the wave penetrates radially into the inhomogeneous plasma.

Since the turbulent diffusion coefficient, $D_\perp$, could not readily be measured, in order to study effects of background turbulence we injected broad-band rf noise into the plasma via grids and looked for an increase in k_{x_i}/k_{x_r}. It was found that the noise affected the coupling efficiency between the slow wave structure and the plasma, and also, large noise levels ($\delta n/n > 10\%$) caused the wave packet to be smeared out radially. These two effects can reduce the wave amplitude at a given radial position but do not provide clear evidence of dissipative energy loss by the wave packet (i.e., an increase in the spatial e-folding of the wave amplitude). However, turbulent damping is expected to be large only when k_x is large; i.e., when ω is close to the lower hybrid frequency. In our experiment it was not possible to avoid strong Landau damping as $\omega \to \omega_{lh}$, and hence, we concluded that density fluctuation turbulence was not the dominant damping mechanism here. However, as mentioned previously, the injected noise could strongly attenuate interferometer signals by enhancing the phase decorrelation of the waves.

V. SUMMARY AND CONCLUSIONS

In order to describe externally excited electrostatic lower hybrid waves, it is necessary to take into account the detailed Fourier spectrum of the antenna. When this is done, it is found that only a source periodic in the z direction will excite waves having well defined k_z and k_x. This type of source excites a spatial wave packet which propagates along a conical trajectory, making a small angle $[\theta \approx \omega/\omega_{pe} \approx (m_e/m_i)^{1/2}]$ with respect to the confining magnetic field.[10]

In order to make quantitative measurements of these waves, it is important to have a plasma with minimal density fluctuations because these fluctuations can cause a phase decorrelation of the wave along its trajectory, making interferometry difficult or impossible.

Using a periodic source designed to have a suitable k_z spectrum, we have excited lower hybrid waves having well defined parallel and perpendicular wavelengths. We have verified the conical propagation of the spatial wave packet excited by this source, and also, using sampling techniques, have shown that the wave is a backward wave. We have found that in the presence of axial density gradients k_z increases as the wave propagates axially into regions of decreasing density. (This is the opposite of the behavior of k_x in the presence of radial density gradients.) By varying the generator frequency, ω, and measuring k_x and k_z, we have verified the cold plasma lower hybrid dispersion relation.

Because of the possibility of phase decorrelations occurring, measurements of wave damping cannot be made from the spatial e folding of the interferometer signal envelope. Instead, damping rates must be measured directly from the e folding of the detected wave amplitude. One must use more precautions to eliminate spurious signals with this technique than is necessary when using interferometry. Externally injected noise increases the instrumental damping caused by phase decorrelation of interferometer signals but does not increase the spatial e folding of the wave amplitude. Instead, in the present experimental regimes ($\omega/\omega_{lh} \gtrsim 1.5$), the injected noise changes the coupling from the antenna to the plasma and also causes a radial smearing out of the wave packet without greatly changing the total energy in the wave packet.

The experimentally determined spatial damping ratio k_{x_i}/k_{x_r}, with k_{x_i} measured from the e folding of the wave amplitude and k_{x_r} from the interferometer signal, is in reasonable agreement with electron Landau damping, provided the electron distribution function is assumed to contain an approximately 30% high energy ($\approx 15-30$ eV) tail.

In conclusion, we have shown that, by using a periodic slow wave antenna, it is possible to excite well defined lower hybrid waves and that the experimentally observed characteristics of these waves are in good agreement with theory. However, because of strong electron Landau damping before the wave could reach the lower hybrid layer, linear mode conversion into hot ion plasma waves was not observed.

ACKNOWLEDGMENTS

We would like to thank J. Johnson and J. Taylor for their technical assistance.

We would also like to thank Dr. J. P. M. Schmitt for having initiated the construction of the multiple filament plasma source.

One of the authors (P.B.) would like to thank the National Research Council of Canada for having provided him with financial support during the course of this work.

This work was supported by U. S. Energy Research and Development Administration Contract E(11-1)-3073. Use was made of computer facilities supported in part by National Science Foundation Grant NSF-GP579.

[1]T. H. Stix, *The Theory of Plasma Waves* (McGraw-Hill, New York, 1962), Chap. 3.
[2]V. E. Golant, Zh. Tekh. Fiz. **41**, 2492 (1971) [Sov. Phys.—Tech. Phys. **16**, 1980 (1972)].
[3]T. H. Stix, Phys. Rev. Lett. **15**, 878 (1965).
[4]H. H. Kuehl, Phys. Fluids **5**, 1095 (1962).
[5]R. K. Fisher and R. W. Gould, Phys. Fluids **14**, 857 (1971).

[6]J. Dawson and C. Oberman, Phys. Fluids **2**, 103 (1959).
[7]R. J. Briggs and R. R. Parker, Phys. Rev. Lett. **29**, 852 (1972).
[8]W. M. Hooke and S. Bernabei, Phys. Rev. Lett. **28**, 407 (1972).
[9]P. L. Colestock and W. D. Getty, in *Proceedings of the Second Topical Conference on RF Plasma Heating* (Texas Tech University, Lubbock, Tex., 1974), paper B3.
[10]P. Bellan and M. Porkolab, Phys. Fluids **17**, 1592 (1974).
[11]P. Bellan and M. Porkolab, Phys. Rev. Lett. **34**, 124 (1975).
[12]T. H. Dupree, Phys. Fluids **10**, 1049 (1967).
[13]H. Okuda and J. M. Dawson, Phys. Fluids **16**, 408 (1973).
[14]C. Chu, Ph.D. thesis, Princeton University (1974).
[15]B. Grek, Ph.D. thesis, Princeton University (1975).
[16]W. Gekelman and R. L. Stenzel, Rev. Sci. Instrum. **46**, 1386 (1975).
[17]G. Lisitano, M. Fontanesi, and E. Sindoni, Appl. Phys. Lett. **16**, 122 (1970).
[18]B. Grek and M. Porkolab, Phys. Rev. Lett. **30**, 836 (1973).
[19]R. P. H. Chang and M. Porkolab, Phys. Rev. Lett. **32**, 1227 (1974).
[20]J. G. Laframboise, University of Toronto, Institute for Aerospace Studies Report 100 (1966).
[21]P. E. Vandenplas, in *Symposium on Plasma Heating and Injection* (Edatrice Compositori, Bologna, Italy, 1972), p. 101.